Simulation of Rotary Motion Generated by Head-to-Head Carbon Nanotube Shuttles

Mustapha Hamdi, Arunkumar Subramanian, Lixin Dong, Antoine Ferreira, Bradley J.Nelson

Simulation of Rotary Nanomotions Based on Head-to-Head Carbon Nanotube Shuttles

Mustapha Hamdi, Arunkumar Subramanian, Lixin Dong, *Member, IEEE,* Antoine Ferreira, *Member, IEEE,* Bradley J. Nelson, *Senior Member, IEEE*

***Abstract*—A novel rotary nanomotor is described using two axially aligned, opposing chirality nanotube shuttles. Based on inter-shell screw-like motion of nanotubes, rotary motion is generated by electrostatically pulling the two cores together. Simulations using molecular dynamics show the generation of rotation from armchair nanotube pairs and their actuation properties. The simulation results, point towards the use of these motors as building blocks in nanoelectromechanical systems (NEMS) and nanorobotic systems for sensing, actuation, and computation applications.**

***Index Terms*—Rotary nanomotor, nanotube, NEMS, nanorobotic system, molecular dynamics simulation.**

I. Introduction

Since the discovery of carbon nanotubes (CNTs) [1], researchers have identified a number of promising applications in nanoelectronics, nanosensing [2b], nanoelectromechanical systems (NEMS) [2c], and nanorobotic systems [2] based on their unique electrical and mechanical properties. The atomic smooth surfaces and weak van der Waals interactions between nanotube shells allow them to readily slide and rotate relative to each other. Previous reports on the inter-shell interactions and electrostatic actuation of telescoping multiwalled carbon nanotubes (MWNTs) [3-5] have demonstrated the robustness of these nanostructures. In these structures, motion at the nanometer scale can be generated in the form of sliding, rotation or screw-like motion between nanotube walls. Devices that have been proposed based on these forms of motion include bearings [3, 6, 7, 7b], linear servomotors with integrated position sensing [4], resonators/oscillators [8, 9], encoders [7], and electrical switches [10]. Experimental [11, 12] and computational [13, 14] investigations have also been performed on the geometric and energetic parameters that characterize the relative position and motion of the neighboring walls of a nanotube for rotational nanoactuators. In experimentally demonstrated devices [11, 12], nanotubes served as bearings for a nanometallic rotor, which is electrostatically actuated using microfabricated stator electrodes [11].

The chiral structures of nanotube shells [14, 15] offer alternate possibilities for generating rotary motion between coaxial nanotube shells without involving extra rotors. In another effort, a rotary motor [16] was conceptually constructed from a double-walled carbon nanotube (DWNT) consisting of two single-walled carbon nanotubes (SWNTs) with different length and chirality within the framework of the Smoluchowski-Feynman ratchet. In that design, the axial sliding motion of the inner tube has been assumed to be constrained and unidirectional rotation has been shown in the presence of a varying axial electrical voltage. Here we propose an electrostatic rotary nanomotor based on two axially aligned nanotube shuttles, where the axial sliding motion can be constrained by the two nanotubes against each other. In addition, our recent success on the batch fabrication of shell engineered nanotubes has demonstrated the key processes required to construct such shuttles for the first time [6]. The presented technique also offers a powerful tool to control the degrees of freedom of MWNT nanoconstructs, which is essential in a number of nanorobotic/nanomanipulation applications.

In order to reduce the development cost and time during the nanodevice prototyping, computational methods of simulation are used in this work to palliate the lack of measurement data. We present molecular dynamics (MD) simulations coupled to an adaptive intermolecular REBO AIREBO potential and electrostatic interactions to characterize a supermolecular nanomotor. The goal of the present work is to theoretically demonstrate its working principle and characterize their actuation properties by considering the combination of chilarity pairs and their mutual, non-bonded atomic interactions. MD-based computations are used to extract device performance characteristics like inter-shell and inter-segment interaction energies, rotation, friction and oscillation that relies on rotational motion between individual shells of a multiwalled carbon nanotube.

Manuscript received February 12, 2011.
The content of this paper has been partially presented at the IEEE International Conference on Robotics and Automation (ICRA2010), Anchorage, Alaska, May 3 -8, 2010.

M. Hamdi and A. Ferreira are with the Laboratoire PRISME, Ecole Nationale Supérieure de Bourges, Bourges, 88 Boulevard Lahitolle, 18000 Bourges, France (phone: +33 2 4848 4079; e-mail: mfhamdi@gmail.com, antoine.ferreira@ensi-bourges.fr).

A. Subramanian, L. X. Dong, and B. J. Nelson are with the Institute of Robotics and Intelligent Systems, ETH Zurich, 8092 Zurich, Switzerland (phone: +41-44-632-2539; fax: +41-44-632-1078; e-mail: bnelson@ethz.ch). A. Subramanian is currently with Center for Integrated Nanotechnologies, Sandia National Laboratories, Albuquerque, NM 87185, USA (e-mail: asubram@sandia.gov). L.X. Dong is currently with the Department of Electrical & Computer Engineering, Michigan State University, East Lansing, MI 48824-1226, USA (e-mail: ldong@egr.msu.edu).

The outline of the paper is as follows. The design and fabrication of the rotary nanotube motors is proposed in Section 2. In Section 3, the coupling of molecular dynamics and electrostatic charge distribution is introduced. Then, the mechanical characterization of nanomotor actuation, including nonlinear characteristics of electrostatic forces, motion trajectory, friction and hysteresis, are discussed in Section 4, followed by the conclusions..

II. Design and Fabrication of Rotary Nanotube Motors

The rotary nanomotor is schematically illustrated in Fig. 1 (a) and (b). The motor consists of two MWNT segments with opposing chiralities. The outermost shells are fixed and the inner shells are freely suspended inside the outer ones. By applying a DC actuation voltage between the segments, the axially aligned inner tubes approach each other due to electrostatic forces. Due to their opposite chiralities, both sliding and rotation, i.e., a nanoscrew, will be generated simultaneously during this motion. The chiral layers in an MWNT form a bolt-nut pair, and the ultra-small interlayer friction resembles that in a lead-screw (Fig. 1(a)). These make it possible to form a bolt-nut based nanomotor when we put two pairs with opposite chirality and actuate them electrostatically in a non-contact way. After contact is made, the sliding motion will be constrained, whereas rotation will remain as the only possible degree-of-freedom for motion.

One possible route towards fabricating these nanostructures involves picking CNTs with opposing chiralities and placing them head-to-head using nanorobotic manipulation [2]. More recently, we have reported an alternate approach that realizes batch fabricated nanoshuttles using a combination of dielectrophoretic nanoassembly and high-yield, current-driven shell engineering processes [3, 6, 7]. In this approach, an individual MWNT is assembled onto multiple, electrically isolated electrodes. The NT segments between electrodes are then vaporized using the current-driven shell-etching technique (Fig. 1 (c) and (d)). Multiple, capless nanotube segments with a 220-nm pitch and 6 to 15nm spacing are created from a single nanotube using this method, which is outlined in detail in [3, 6, 7]. Since a single nanotube is broken into multiple, axially aligned segments with this approach, the requirement of creating nanoshuttles with opposing chiralities can be met only in the case of armchair nanotubes, where the helical angle can be regarded as either $\pi/6$ or $-\pi/6$. The rotational direction in the case of armchair nanotube pairs cannot be predetermined in theory, but the motor is expected to initiate rotation in one direction based on a random dynamic factor and further continue this unidirectional rotation. Thus, an important requirement for the use of this batch fabrication approach for realizing nanoshuttles outlined in this paper is that the nanotube sample, which is used for dielectrophoretic assembly, should contain only armchair nanotubes. While challenges remain in controlling the chirality of individual nanotubes, recent progress on this aspect of nanotube growth such as forming MWNTs with every shell having a zigzag helicity [17] and armchair SWNTs [18, 19] offer promising routes towards realizing all-armchair CNTs as required for the

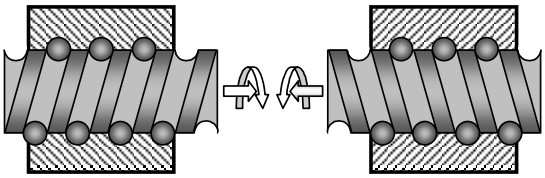

(a)

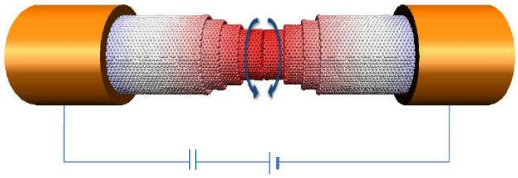

(b)

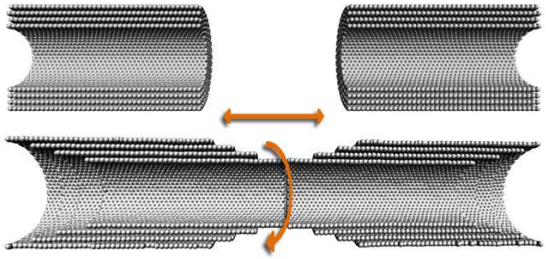

(c)

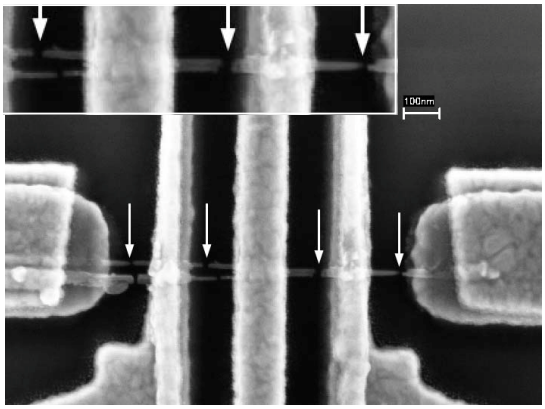

(d)

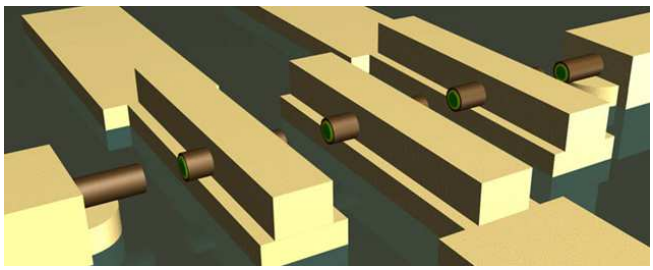

(e)

Fig. 1. (a) Operating principle and (b) schematic design of a rotary nanomotor based on axially aligned nanotube shuttles. The voltage is applied to both sides with a direct current voltage in series with a capacitor to avoid the generation of current. (c) Cross-section view of the rotary nanomotor. (d) Shell engineered nanotube shuttles formed with a 220 nm pitch and separated by ~10 nm gaps. The arrows point to the inter-segment gaps in this image. (e) Schematic illustration of the core–shell mechanism with the inter-segment gaps exaggerated to reveal the shell structure.

batch fabrication approach.

III. Molecular Dynamics Simulations on Rotary Motors

Since the nanotube wall has a helical symmetry, it was recently proposed that a DWNT can serve as a nanoscrew. Such nanoscrews can operate, for example, as an auger of a perforating nanodrill or a nanodevice in which a force or linear motion along the nanotube axis can be transformed into a torque or rotary motion of the core tube [16]. Previously, a classification scheme for non-chiral DWNTs has been developed [13], energetic barriers to the relative sliding and rotation of walls in DWNTs [14] and to the rotation of shells in double-shell nanoparticles[15, 16] have been calculated, and the theory for dynamics of the relative rotation, sliding and screw like motion of nanotube walls has been developed [14]. In this work, we show by molecular dynamics simulation that it is possible to construct a MWNT motor actuated by a

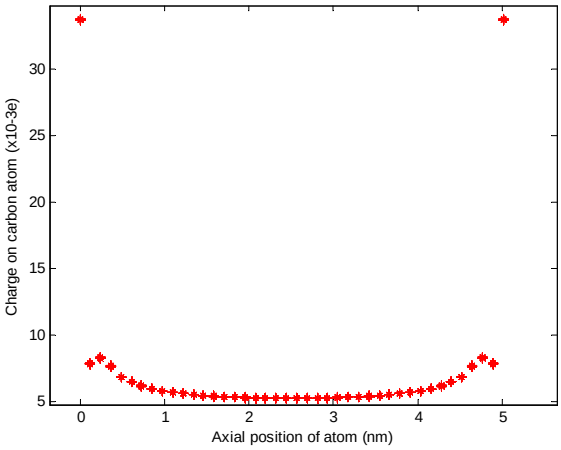

(a)

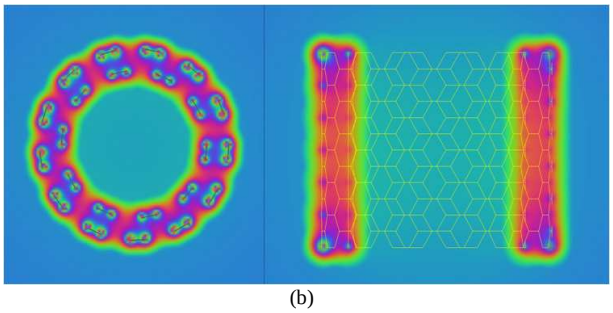

(b)

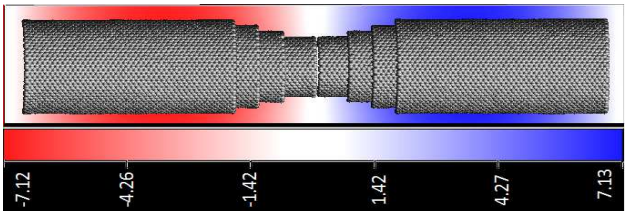

(c)

DC voltage. Without losing generality, the molecular dynamics modeling and the working principle of the motor are

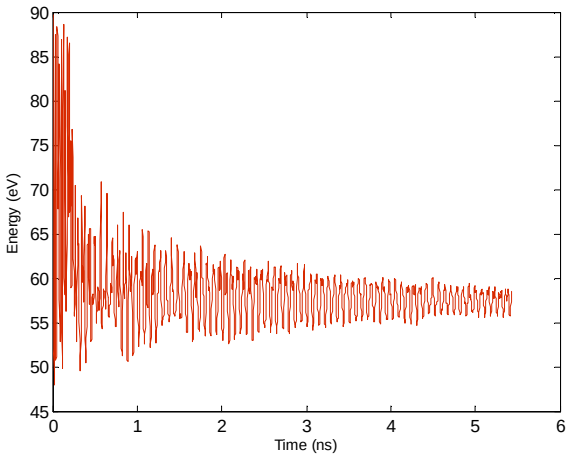

(d)

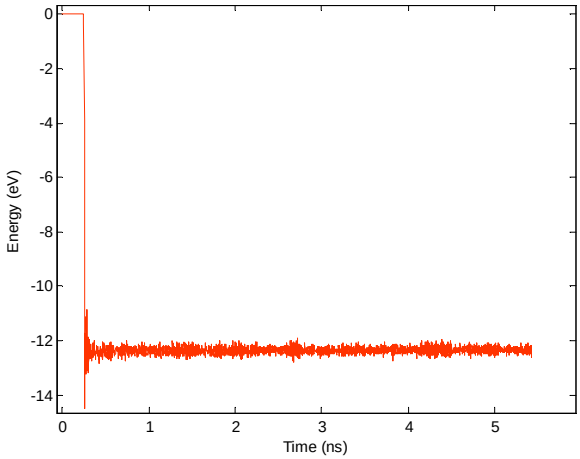

(e)

Fig. 2. (a) Charge distribution along the axial direction for an open ended nanotube (V=6V). (b) Electrostatic potential map along a DWNT structure. (c) Cross-sectional view showing the charge distribution during contact between neighboring segments. Negatively charged shells are located on the left, while the positively charged shells are located on the right. (d) Attractive electrostatic energy between two oppositely charged inner shells. (e) Repulsive electrostatic energy between the inner and outer shells. The sliding time of the system is 0.4ns.

investigated in this paper by taking a rotary motor consisting of two armchair nanotubes as an example. The motor consists of a shuttle structure as shown in Fig. 1 (a) and (b) with CNT's characteristics given in Table 1. Using classical molecular dynamics with empirical potentials, we show that the inner CNT can rotate.

A. Simulation method

In this work, we focus on simulating the nanotube rotary motor's performance using classical means. This approach can consider structures that have dimensions comparable to the experimentally observed ones that have been highlighted in Fig. 1(c) and (d). Specifically, we have considered a 10-shell MWNT device with individual segments that are 200nm long and separated by a gap of 5nm. First, we apply an actuation bias and calculate the charge distribution along the carbon structure using the atomistic moment method. This atomic charge distribution and nanoshuttle structure serve as inputs to the molecular dynamics computations using an adaptive

intermolecular REBO AIREBO potential [20] and electrostatic interactions. MD-based computations are used to extract device performance characteristics like inter-shell and inter-segment interaction energies, rotation, friction and oscillation.

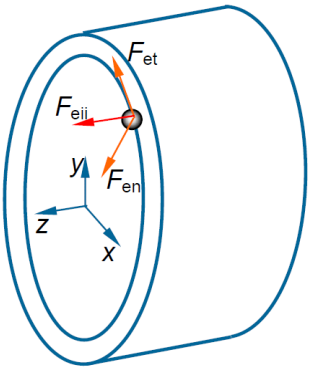

(a)

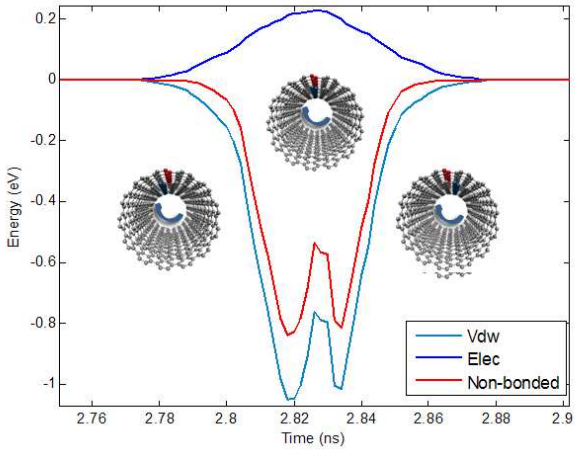

(b)

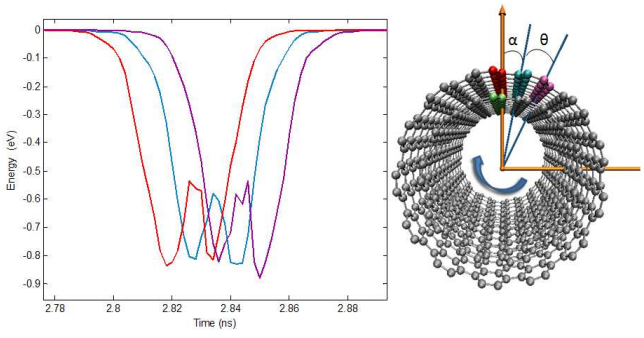

(c)

Fig. 3. (a) Forces acting on a terminus atom located within an inner shell. F_{eii} is the attractive electrostatic force between oppositely charged inner shells located within the neighboring segments. F_{et} and F_{en} are tangential and normal components, respectively, applied by the outer shell within the same nanotube segment. (b) Interaction energies between the two segments in inner and outer shells. Blue, cyan and red curves represent electrostatic, van der Waals and the total non-bonded energy components, respectively. (c) Total non-bonded energy attraction between a segment with green color in the inner nanotube and three successive segments in the outer nanotube.

Table 1 Parameters of CNTs

Shell's number	Chiral angle rd	Chirality vector (n, m)	Diameter 10^{-9}m
Shell 4 (outer)	± π/6	n=m=40	5,424
Shell 3	± π/6	n=m=35	4,746
Shell 2	± π/6	n=m=30	4,068
Shell 1 (inner)	± π/6	n=m=25	3,390

The total potential energy of system is given by $U^{tot} = U^{elec} + U^{P}$, where U^{elec} is the electrostatic energy due to extra charges on two carbon atoms and U^{P} is the AIREBO interatomic potential. AIREBO potential introduces non-bonded interactions through an adaptive treatment, which allows the reactivity of the REBO potential to be maintained. A possible problem due to the introduction of intermolecular interactions is that the repulsive barrier between non-bonded atoms may prevent chemical reactions from occurring. The AIREBO potential corrects this problem by modifying the strength of the intermolecular forces between pairs of atoms depending on their local environment. The AIREBO potential term [20] is given by:

$$U^{P} = \frac{1}{2}\sum_{i=1}^{N}\sum_{\substack{j=1 \\ i\neq j}}^{N}\left[\varphi^{R}\left(r_{i,j}\right) - b_{i,j}\varphi^{A}\left(r_{i,j}\right) + \varphi^{LJ}\left(r_{i,j}\right) + \sum_{\substack{k=1 \\ k\neq i,j}}^{N}\sum_{\substack{l=1 \\ l\neq i,j}}^{N}\varphi_{kijl}^{tor}\right] \quad (1)$$

where $\varphi^{R}\left(r_{i,j}\right)$ and $\varphi^{A}\left(r_{i,j}\right)$ are the interatomic repulsion and attraction terms, $\varphi^{LJ}\left(r_{i,j}\right)$ is the parameterized Lennard-Jones potential, $b_{i,j}$ is the bond order function, and φ_{kijl}^{tor} is the single bond torsional interaction. The electrostatic energy is calculated using Coulomb's law: $E_{ij}^{q} = \frac{q_i q_j}{4\pi\varepsilon R_{ij}}$, where q_i and q_j are extra charges on carbon atoms, R_{ij} is the interatomic distance, and ε is the permittivity.

B. Electrostatic charge distribution along the length of a carbon nanotube

Electron microscopy provides direct evidence for inter-shell displacements induced by electrostatic actuation [3, 4]. In our simulations, the charge distribution on the carbon nanotube is obtained by an atomistic moment method based on classical electrostatics theory [21]. We consider MWNTs with finite lengths. For simplicity, the nanotube is assumed to be situated in an idealized electric field, i.e., the voltage on the nanotube surface is V_0. For a nanotube with N atoms, the potential at an arbitrary atomic position [21] is given by :

$$V\left(r_i\right)=\sum_{j=1}^{N}\frac{q_j}{4\pi\varepsilon_0\left|r_i-r_j\right|} \quad (2)$$

where V is the electric potential, q_j the point charge on atoms, r_i the location of the charged atom, and ε_0 the permittivity of vacuum. Because of the equipotential status of the nanotube surface, N equations can be written in a matrix form as follows:

$$[A]\{q\}=\{V\} \quad (3)$$

where $\{q\}$ and $\{V\}$ are the charge vector and the potential vector, respectively, and $[A]$ is an N×N matrix.

Using Density Function Theory (DFT) we calculated the charge redistribution along double walled nanotube [22 23]. We found that electrons are transferred from outer tube to the inner tube with charge transfer density of 0.002 e/Å.

IV. Results and Discussions

A. Nanomotor actuation

For structures with geometric parameters similar to those illustrated in Fig. 1(c) and (d), simulations establish that the MWNT shuttle-based devices can be actuated electrically, and the neighboring segments slide towards each other to come in contact at low voltages (~ 5V). In this effort, we have specifically investigated the rotation of inner shells in this contact state.

To explain the proprieties of nanomotor behavior, intershell electrostatic and van der Waals energies were investigated and inner CNT trajectories were studied using MD simulations. The charge distribution along the CNTs was calculated as described in section III. Fig. 2(a) shows the charge distribution on carbon atoms along the length of a 5 nm long SWNT when the electric potential on the surface is 6.0 V. The electric charge value is in the range of 5×10^{-3} to 34×10^{-3}e. It can be seen that the charges on atoms located at the central part of the tube do not vary significantly, whereas the charges on atoms at the two ends are much higher. The charge values reach up to 34×10^{-3} e for the open-ended nanotube. Fig. 2(b) shows the electrostatic potential map along a DWNT. In addition, the electrostatic potential is much higher at the outer nanotube as compared to the inner one [22].

When a potential difference is applied between the two MWNT segments, opposite charges are induced on these MWNT segments, as illustrated in Fig. 2(c) where the blue color presents the positive charge and the red color represents the negative charge. The electrostatic interactions due to these induced charges include attractive forces between oppositely charged neighboring MWNT segments and repulsive forces between the same-polarity shells within the individual MWNT segments. For a given bias, the attractive electrostatic energy between two oppositely charged inner nanotubes as a function of time is shown in Fig. 2(d). Fig. 2(e) depicts the repulsive electrostatic energy between the inner and the outer shells. The net effect of these electrostatic interactions due to an applied bias is an electrostatic force that tends to slide the inner shells within the two segments towards each other. When this applied excitation bias exceeds a characteristic threshold value, these electrostatic interactions become higher than the van der Waals forces that try to restrain the inner shells from extruding. This results in a closure of the inter-segment gap. For the system under consideration, the sliding time is 0-0.4 ns. This is comparable to device operation times estimated in [22].

B. Rotation of inner shells

1) Force analysis

At the closed state of the system, a terminus atom within the inner shell is subjected to van der Waals forces and three components of electrostatic forces. Fig. 3(a) shows a terminus carbon atom with these force components. F_{eii} is an attractive electrostatic force which is applied by the inner shell of the neighboring nanotube segment. F_{et} and F_{en} are the tangential and normal components, respectively, of the electrostatic repulsive force applied by the outer shell of the same nanotube segment (N.B. the van der Waals components are not shown in this figure).

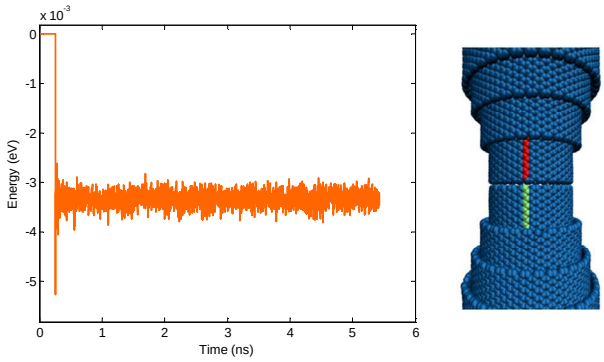

Fig. 4. Attractive electrostatic energy between the inner shells within two neighboring segments (red colored segment and green colored one). As shown by the curve, sliding occurs between 0 and 0.2ns, while at 0.2ns the inner shells establish contact. After 0.2ns, the energy is constant indicating that both inner shells rotate with the same velocity and in the same direction.

In order to understand the origin of this inner shell rotation, we calculate the inter-layer interactions during rotation. We divide the nanotube into unit cells as illustrated in Fig. 3(b). This figure shows the two types of energies acting on an inner unit cell as it approaches an outer one. These two energies are added together to get the total non-bonded energy acting on the inner unit cell. The graph shows that from 2.780ns to 2.818ns, the total attractive non-bonded energy (red curve) increases, and from about 2.833 to 2.900 ns the total energy decreases when the two unit cells become close and separate. At 2.828ns, the non-bonded energy decreases to -0.55eV because of the repulsive van der Waals term when the atoms are very close. This clearly shows that the rotation of the inner nanotubes is mainly caused by the interlayer attractive non-bonded energy.

We characterized the interaction energy between a unit cell in the inner and three successive unit cells in the outer

nanotube during a $\alpha+\beta$ rotation angle. Fig. 3(c) illustrates the interaction between these unit cells.

a) During the time interval between 2.780ns to 2.835ns, the total non-bonded energy between the inner segment (green colored) and the first outer segment (red) significantly increases. This means that the inner segment is strongly attracted by the first outer segment. At 2.828ns, the energy decreases to -0.55eV which is caused by the repulsive van der Waals energy when the neighboring segments become quite close.

b) During the time interval between 2.820ns to 2.848ns, the total non-bonded attractive energy between the inner segments (green) and the second outer segment (cyan) increases strongly. This means that the inner segment is strongly attracted by the first outer segment. At 2.835ns, the energy decreases to -0.55eV which is caused by the repulsive van der Waals energy when the neighboring segments become very close.

c) During the time interval between 2.830 ns to 2.850 ns, the total non-bonded attractive energy between the inner segments (green) and the third outer segment (magenta) increases strongly. That means the inner segment is strongly attracted by the first outer segment. At 2.848ns, the energy decreases to -0.55eV which is caused by the repulsive van der Waals energy when the neighboring segments become close.

The calculations, using MD simulations coupled to electrostatic charge distribution calculations along the CNTs, show that electrostatic forces bring the two segments in contact (Fig. 3(b)). The calculations demonstrate that the interlayer van der Waals forces at the contact state can generate a torque and result in rotation (Fig. 3(c)). Van der Waals forces are stronger than the friction forces during rotation.

The attractive electrostatic energy analysis between head to head CNTs shows that these CNTs rotate with the same velocity and in the same direction, as illustrated in Fig. 4. The attractive electrostatic energy becomes stable after the neighboring segments come in contact with each other. The inner shell trajectory analysis shows rotation with constant velocity as illustrated in Fig. 5.

We studied the mechanical properties of the MWNT shuttle-based device. The mechanical delivered force obtained directly from simulation. We use a modified steered molecular dynamics (SMD) technique to measure the motion force bringing the two segments in contact. We ran a MD simulation of the electrostatic force with an applied external constraint to the inner shell terminus. This constraint was applied in the form of a harmonic spring of known stiffness *k*, attached to the center of mass of the terminus nucleic acid. The harmonic guiding potential and the corresponding exerted force for this system are of the form [24]:

$$U = -k(x - x_0)^2/2 \quad \text{and} \quad F = k(x - x_0). \qquad (4)$$

where x_0 and x are the position at rest and the current position in nm. As shown in the Fig.6, the mechanical delivered force

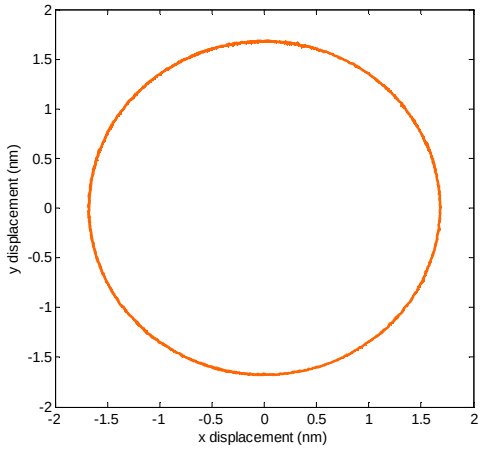

(a)

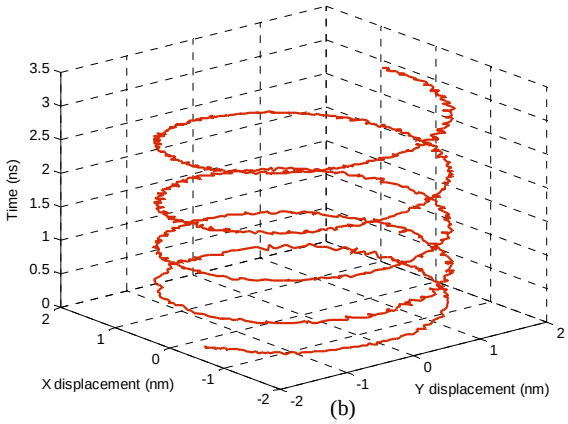

(b)

Fig. 5. Termini atom trajectory in an inner shell during rotation, (a) Rotating circular path of this terminus atom, (b) Terminus atom rotation as a function of time. This curve shows that the inner shell rotates with constant velocity.

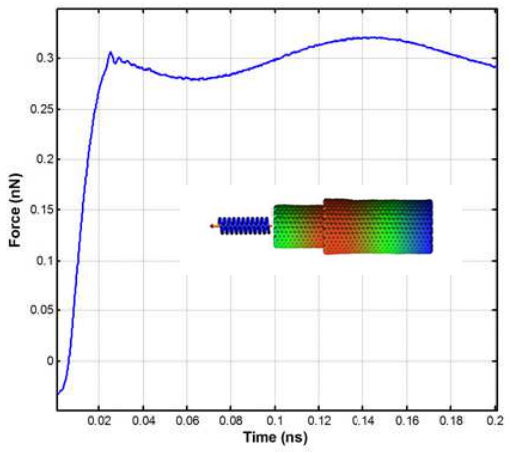

Fig. 6. Termini atom mechanical force in a inner shell delivered during a 10 nm "OFF"-to-"ON" transition. The force is measured by a modified steered molecular dynamics.

varies linearly with a constant slope during its transient state. Then, when both inner tubes are approaching, it is clearly seen that saturation occurs when in contact. The driving force is around a mean value of 0.3 nN.

2) Hysteresis analysis

MD simulations demonstrate the hysteresis behavior by distance-bias plots of the inner CNTs during the increasing and decreasing voltage cycles. Figure 7 represents the hysteresis plot of the MWNT shuttle-based device in which the voltage was first increased from 25 to 37V and, then, decreased from 38 to 25 V (voltage values are not scaled).

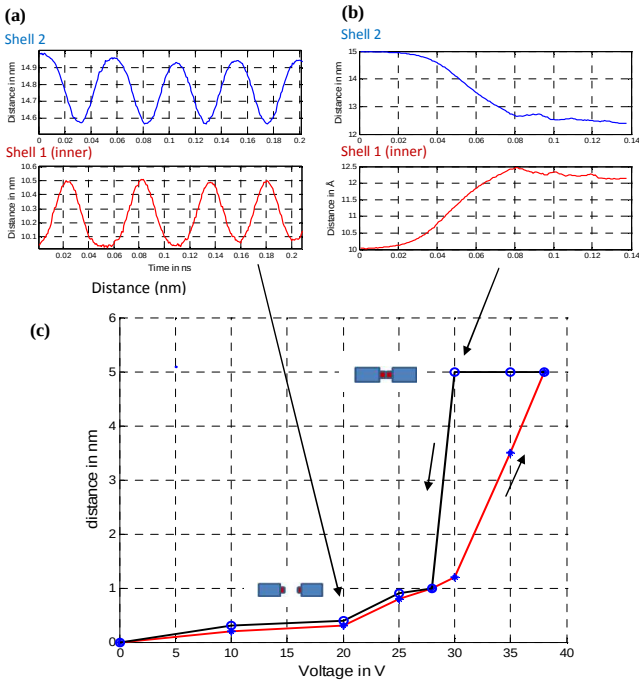

Fig. 7. Hysteresis behavior indicated by distance-bias plots of MWNT shuttle during the increasing and decreasing voltage cycles. Insets show the profiles of center-of-distance separation between shell 1(inner tube), shell 2 and outer tube for "ON"-to-"OFF" transition. (a) a bias between 5-to- 20V generates an oscillatory motion while (b) a bias up to 37V generate the contact state between both inner tubes.

As can be seen from the MD simulation in Fig.7(c), the nanomotor reaches the contact state at 37V during the increasing voltage segment and returns to a non contact state at 30V during the decreasing voltage segment. This characteristic can be attributed to electrostatic forces between the inner shells of that bring the two segments in contact. As demonstrated previously in Fig. 3(b), these forces are a function of both applied voltage as well as shell position. Insets shown in Fig.7(a) and Fig.7(b) demonstrate the transient behavior between oscillatory-to-contact motion. Oscillatory motion, around 20Ghz, is sustained for low bias values below the threshold voltage (30.1V) [25]. We can see that the amplitude of the separation distance keeps constant, and it is equal to the initial extrusion length of the shell 1 (in red) and the shell 2 (in blue). It can be seen that the "OFF"-to-"ON" transition (38V) occurs at a higher voltage compared to the "ON"-to-"OFF" transition (29V). This hysteresis behavior has been exhibited in experimentation by the authors in [26].

V. Conclusions

A rotary nanomotor has been designed using two axially aligned, opposing chirality nanotube shuttles. Based on inter-shell screw-like motion between nanotubes, rotary motion is generated by electrostatically pulling the inner shells together. Simulations using molecular dynamics were used to investigate how rotation from a pair of nested armchair nanotube pairs can be generated. The ultra-compact dimensions compared to previous designs and the progress on batch fabrication of similar nanostructures indicate that these motors are promising building blocks of NEMS and nanorobotic systems for sensing, actuation, and computation applications.

References

[1] S. Iijima, "Helical microtubules of graphitic carbon," *Nature*, vol. 354, pp. 56-58, Nov 1991.

[2] L. X. Dong, A. Subramanian, and B. J. Nelson, "Carbon nanotubes for nanorobotics," *Nano Today*, vol. 2, pp. 12-21, Dec 2007.

[2b] T. Mirfakhrai, J. Oh, M.E. Kozlov, S. Fong, M. Zhang, R.H. Baughman, J.D.W. Madden, "Mechanoelectrical force sensors using twisted yarns of carbon nanotubes", IEEE/ASME Transations on Mechatronics, Vol.16, No.1, Feb.2011, pp.90-97.

[2c] N. Jalili, P.X. Liu, G. Alici, A. Ferreira, "GuestEditorial: Introduction to the Focused Section on Mechatronics for MEMS and NEMS", IEEE/ASME Transations on Mechatronics, Vol.14, No.4, Aug.2009, pp.397-404.

[3] J. Cumings and A. Zettl, "Low-friction nanoscale linear bearing realized from multiwall carbon nanotubes," *Science*, vol. 289, pp. 602-604, Jul 2000.

[4] L. X. Dong, B. J. Nelson, T. Fukuda, and F. Arai, "Towards nanotube linear servomotors," *IEEE Transactions on Automation Science and Engineering*, vol. 3, pp. 228-235, Jul 2006.

[5] A. Kis, K. Jensen, S. Aloni, W. Mickelson, and A. Zettl, "Interlayer forces and ultralow sliding friction in multiwalled carbon nanotubes," *Physical Review Letters*, vol. 97, art. no. 025501, Jul 2006.

[6] A. Subramanian, L. X. Dong, J. Tharian, U. Sennhauser, and B. J. Nelson, "Batch fabrication of carbon nanotube bearings," *Nanotechnology*, vol. 18, art. no. 075703, Feb 2007.

[7] H. Jiang, M. F. Yu, J. Q. Lu, Y. Huang, H. T. Johnson, X. G. Zhang, and P. Ferreira, "Carbon nanotube electronic displacement encoder with sub-nanometer resolution," *Journal of Computational and Theoretical Nanoscience*, vol. 4, pp. 574-577, May 2007.

[7b] L. Dong, F. Arai, T. Fukuda, "Destructive constructions of nanostructures with carbon nanotubes through nanorobotic manipulation", IEEE/ASME Transations on Mechatronics, Vol.9, No.2, June 2004, pp.350-357.

[8] Q. S. Zheng and Q. Jiang, "Multiwalled carbon nanotubes as gigahertz oscillators," *Physical Review Letters*, vol. 88, art. no. 045503, Jan 2002.

[9] K. Jensen, C. Girit, W. Mickelson, and A. Zettl, "Tunable nanoresonators constructed from telescoping nanotubes," *Physical Review Letters*, vol. 96, art. no. 215503, Jun 2006.

[10] V. V. Deshpande, H. Y. Chiu, H. W. C. Postma, C. Miko, L. Forro, and M. Bockrath, "Carbon nanotube linear bearing nanoswitches," *Nano Letters*, vol. 6, pp. 1092-1095, Jun 2006.

[11] A. M. Fennimore, T. D. Yuzvinsky, W. Q. Han, M. S. Fuhrer, J. Cumings, and A. Zettl, "Rotational actuators based on carbon nanotubes," *Nature*, vol. 424, pp. 408-410, Jul 2003.

[12] B. Bourlon, D. C. Glattli, C. Miko, L. Forro, and A. Bachtold, "Carbon nanotube based bearing for rotational motions," *Nano Letters*, vol. 4, pp. 709-712, Apr 2004.

[13] A. V. Belikov, Y. E. Lozovik, A. G. Nikolaev, and A. M. Popov, "Double-wall nanotubes: Classification and barriers to walls relative rotation, sliding and screwlike motion," *Chemical Physics Letters*, vol. 385, pp. 72-78, Feb 2004.

[14] R. Saito, R. Matsuo, T. Kimura, G. Dresselhaus, and M. S. Dresselhaus, "Anomalous potential barrier of double-wall carbon nanotube," *Chemical Physics Letters*, vol. 348, pp. 187-193, Nov 2001.

[15] P. A. E. Schoen, J. H. Walther, S. Arcidiacono, D. Poulikakos, and P. Koumoutsakos, "Nanoparticle traffic on helical tracks: Thermophoretic mass transport through carbon nanotubes," *Nano Letters*, vol. 6, pp. 1910-1917, Sep 2006.

[16] Z. C. Tu and X. Hu, "Molecular motor constructed from a double-walled carbon nanotube driven by axially varying voltage," *Physical Review B*, vol. 72, art. no. 033404, Jul 2005.

[17] M. Kusunoki, T. Suzuki, C. Honjo, T. Hirayama, and N. Shibata, "Selective synthesis of zigzag-type aligned carbon nanotubes on sic (000-1) wafers," *Chemical Physics Letters*, vol. 366, pp. 458-462, Dec 2002.

[18] J. M. Cowley, P. Nikolaev, A. Thess, and R. E. Smalley, "Electron nano-diffraction study of carbon single-walled nanotube ropes," *Chemical Physics Letters*, vol. 265, pp. 379-384, Feb 1997.

[19] A. Kasuya, Y. Sasaki, Y. Saito, K. Tohji, and Y. Nishina, "Evidence for size-dependent discrete dispersions in single-wall nanotubes," *Physical Review Letters*, vol. 78, pp. 4434-4437, Jun 1997.

[20] S. J. Stuart, A. B. Tutein, and J. A. Harrison, "A reactive potential for hydrocarbons with intermolecular interactions," *Journal of Chemical Physics*, vol. 112, pp. 6472-6486, Apr 2000.

[21] C. Y. Li and T. W. Chou, "Theoretical studies on the charge-induced failure of single-walled carbon nanotubes," *Carbon*, vol. 45, pp. 922-930, Apr 2007.

[22] V. Zólyomi, J. Koltai, Á. Rusznyák, J. Kürti, Á. Gali, F. Simon, H. Kuzmany, Á. Szabados, and P. R. Surján, "Intershell interaction in double walled carbon nanotubes: Charge transfer and orbital mixing," *Physical Review B*, vol. 77, art. no. 245403, 2008.

[23] Y. Miyamoto, S. Saito, and D. Tomanek, "Electronic interwall interactions and charge redistribution in multiwall nanotubes", *Physical Revew B*, vol. 65, art. no. 041402, 2002.

[24] Hamdi M, Sharma G, Ferreira A and Mavroidis D, "Prototyping bio-nanorobots using molecular dynamics simulation and virtual reality *Microelectron. J.* **39** 190–201, 2008.

[25] S. Xiao, W. Hou, "Studies of nanotube-based resonant oscillators through multiscale modeling and simulation", *Physical Review B*, 75, 125414, 2007.

[26] A. Subramanian, L.X. Dong, B.J. Nelson, A. Ferreira, "Supermolecular switches based on multiwalled carbon nanotubes", *Applied Physics Letters*, 96, 073116, 2010.